Simulating the Lipkin-Meshkov-Glikov model on a classical computer

Grzegorz Kajda
Bachelor Student, Robotics and Intelligent Systems
Department of Informatics The faculty of Mathematics and Natural Sciences
Email: grzegork@ifi.uio.no

1 Abstract

We present a comprehensive simulation of the simplified Hamiltonian of the Lipkin-Meshov-Glikov (LMG) model on a classical computer, employing the Variational Quantum Eigensolver (VQE) algorithm. Initially, we explore the outcomes arising from the application of diverse single qubit quantum gates to one qubit systems prepared in basis states. Following that, an entangler circuit is constructed, and one of the four bell pairs is prepared, to which we apply the Hadamard and CNOT gates. Utilizing our newfound grasp of the foundational principles governing quantum systems, we construct quantum circuits for generating ansatz states and methodically develop the VQE from ground up.

To assess the VQE's efficiency, we apply it to quantum systems representing single and two-particle systems, comparing its performance against an analytical solver. Transitioning to the Lipkin model, we leverage the properties of annihilation and creation operators to reformulate the Lipkin model's Hamiltonian first in terms of the quasi-spin operator and then Pauli operators. Employing this encoding scheme, we apply the VQE to the Lipkin model with spin J=1 and 2, corresponding to situation when the model comprises two and four fermions, respectively. We compare the results against exact solutions obtained through standard diagonalization method. This analysis provides valuable insights into the performance and accuracy of the VQE approach in tackling the Lipkin model's Hamiltonian.

2 Introduction

Since its emergence in the early 1900s, quantum mechanics has sparked fervent discussions among physicists, engaging luminaries of modern physics like Einstein, Dirac, Bohr, and many others. The discovery of the quantum realm profoundly reshaped our perspective and understanding of the world around us, unveiling a whole new realm of fundamental principles governing the very building blocks of the universe. With the advent of computer systems in the latter half of the 20th century, and the introduction of the quantum Turing machine in 1980, the field of quantum computing was born, ultimately leading to the construction of the first quantum computer in 1998. Recently, due to technological advances and discovery of new quantum algorithms, we have been granted to an extent, the capability of simulating simple many-body quantum models using classical computers.

An emerging research area in quantum computing focuses on the simulation of nuclear physics, leveraging the unique properties of quantum systems. Nuclear systems possess distinct characteristics that make them well-suited for exploration using quantum computers, providing insights into particle interactions. However, it is worth noting that quantum computers still face challenges, such as larger error rates compared to classical computers and vulnerability to noise, which can make working with them potentially difficult. Although the field of quantum computing is expanding rapidly, widespread accessibility remains limited, with companies like IBM offering only restricted access to their quantum technology. In light of these factors, we will employ a classical computer to simulate and analyze the simplified Lipkin-Meshkov-Glick model, showcasing the potential that quantum computing holds while acknowledging the current limitations in accessibility.

To facilitate our simulations, we will begin by constructing quantum circuits using single-qubit quantum gates. This approach will allow us to implement the Variational Quantum Eigensolver (VQE) algorithm effectively, enabling us to approximate the ground state energy of the Lipkin model for systems composed of two and four particles.

Apart from the introduction, this paper is organized into four sections. In Section Two, we will provide a comprehensive description of the theory and methods employed in this study. Following that, we will present our results, and finally, conclude with a summary of our findings.

3 Section II: Theory and Method

3.1 Quantum gates

The primary distinction between classical computers and their quantum counterparts lies in the nature of the data they process. On a classical computer, the fundamental data unit is the binary digit, commonly known as a bit, which represents different voltage levels associated with low and high states, or 0 and 1 as is also common.Quantum computers on the other hand, utilize particles as the information unit, hence leading to a fundamentally different approach to data handling. The unique properties of atoms and the underlying principles of quantum mechanics prevent us from treating them in the same manner as classical bits. For instance, in classical computing, logical gates like *and*, *or*, *xor*, and *nand* are commonly used for data processing, but these gates produce irreversible outcomes. However, on quantum computers, irreversible outcomes are generally not allowed, except in the case of measurement.

On a quantum computer, the fundamental data type used for storing information is the *qubit*, which represents the digital manifestation of the wave function for a quantum particle. The principles of quantum mechanics dictate that the evolution of a quantum system can be mathematically described using unitary operators. This implies that the operations applied to quantum systems are inherently reversible. As a result, data processing on a quantum computer necessitates the use of reversible operators, enabling the "uncomputation" of the outcomes produced by quantum gates. The most basic of these operators are typically represented using 2x2 matrices. While these 2x2 operators quantum gates operate on individual qubits, by utilizing the Kronecker product (tensor product), we can in theory construct gates for quantum systems composed of arbitrary number of qubits. In practice we will often find ourselves restricted to at most 8 or 10 qubits before the computational overhead becomes too high.

The following are the basic quantum gates which we will utilize to contruct more complex gates and ciruits:

I. Identity gate

This gate does nothing to the state of the qubit, as if a gate never was applied to the qubit in the first place. Presented below is the matrix representation of the quantum gate the result of applying it to a single qubit:

$$I = \begin{pmatrix} 1 & 0 \\ 0 & 1 \end{pmatrix}.$$

$$H \begin{pmatrix} \alpha \\ \beta \end{pmatrix} = \begin{pmatrix} 1 & 0 \\ 0 & 1 \end{pmatrix} \begin{pmatrix} \alpha \\ \beta \end{pmatrix} = \begin{pmatrix} \alpha \\ \beta \end{pmatrix}$$

II. Pauli-X gate

The Pauli-X gate, also known as the quantum NOT-gate, flips the probability amplitudes α and β, meaning that these values swap place in the state vector. Presented below is the matrix representation of the quantum gate the result of applying it to a single qubit:

$$X = \begin{pmatrix} 0 & 1 \\ 1 & 0 \end{pmatrix}.$$

$$H \begin{pmatrix} \alpha \\ \beta \end{pmatrix} = \begin{pmatrix} 1 & 1 \\ 1 & -1 \end{pmatrix} \begin{pmatrix} \alpha \\ \beta \end{pmatrix} = \begin{pmatrix} \beta \\ \alpha \end{pmatrix}$$

III. Pauli-Y gate

The action of the Pauli Y gate can be described as the mapping of $|0>$ to $i|1>$ and $|1>$ to $i0>$. The action of the gate can also be viewed as a rotation of the state of the qubit around the y-axis of the Bloch sphere (*see Fig.1*) by 180 degrees. Presented below is the matrix representation of the quantum gate the result of applying it to a single qubit:

$$Y = \begin{pmatrix} 0 & -i \\ i & 0 \end{pmatrix}.$$

$$H\begin{pmatrix}\alpha\\ \beta\end{pmatrix} = \frac{1}{\sqrt{2}}\begin{pmatrix}0 & -i\\ i & 0\end{pmatrix}\begin{pmatrix}\alpha\\ \beta\end{pmatrix} = \frac{1}{\sqrt{2}}\begin{pmatrix}-i\beta\\ i\alpha\end{pmatrix}$$

IV. Pauli-Z gate

The Pauli Z gate flips the phase of $|1>$ to $-|1>$ while leaving $|0>$ unchanged, meaning it flips the relative phase of the qubit. Presented below is the matrix representation of the quantum gate the result of applying it to a single qubit:

$$Z = \begin{pmatrix}1 & 0\\ 0 & -1\end{pmatrix}.$$

$$Z\begin{pmatrix}\alpha\\ \beta\end{pmatrix} = \begin{pmatrix}1 & 0\\ 0 & -1\end{pmatrix}\begin{pmatrix}\alpha\\ \beta\end{pmatrix} = \begin{pmatrix}\alpha\\ -\beta\end{pmatrix}$$

V. Hadamard gate

The result of applying the Hadamard gate to either $|0>$ or $|1>$ is a qubit in a super position of both states, with both the basis states having a 50% of occuring. The result is the exactly the same, independent of which of the basis states the qubit is prepared in.

$$H = \frac{1}{\sqrt{2}}\begin{pmatrix}1 & 1\\ 1 & -1\end{pmatrix}.$$

$$H\begin{pmatrix}\alpha\\ \beta\end{pmatrix} = \frac{1}{\sqrt{2}}\begin{pmatrix}1 & 1\\ 1 & -1\end{pmatrix}\begin{pmatrix}\alpha\\ \beta\end{pmatrix} = \frac{1}{\sqrt{2}}\begin{pmatrix}\alpha+\beta\\ \alpha-\beta\end{pmatrix}$$

VI. Phase gate

The Phase gate, when applied to a qubit, represent the rotation of the second part of a qubit state vector corresponding to $|1>$ by 90 degrees around the z-axis of the bloch sphere.

$$S = \begin{pmatrix}1 & 0\\ 0 & i\end{pmatrix}.$$

$$S\begin{pmatrix}\alpha\\ \beta\end{pmatrix} = \begin{pmatrix}1 & 0\\ 0 & i\end{pmatrix}\begin{pmatrix}\alpha\\ \beta\end{pmatrix} = \begin{pmatrix}\alpha\\ i\beta\end{pmatrix}$$

For a single qubit, application of each of these matrices represents a rotation of the qubit on the *Bloch sphere (Fig. 1)*. (For more details, take a look at [Hundt, p.56] or [Nielsen, p.19])

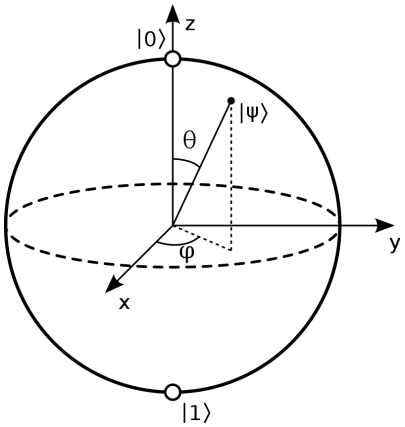

Fig. 1: Three dimensional sphere, known as the Bloch sphere, used to visualize the state of a qubit and the action each quantum gate has on the state vector of the qubit.

VII. CNOT-gate

The Controlled-NOT gate, often abbreviated as CNOT, is a more complex gate that combines the Identity and Pauli-X gates using a Kronecker product. This gate is designed to operate on quantum systems composed of two qubits rather than a single qubit. The name of the gate provides a clue about its functionality. By using the first qubit as a control signal, the CNOT gate flips the amplitudes of the second qubit if the control qubit is in the basis state $|1>$, which corresponds to an active high signal in classical computing. However, if the control qubit is in the state $|0>$, no changes are applied to the second qubit. The specific gate we are discussing here is the $CNOT_{0,1}$-gate, where the first qubit serves as the control signal. It's important to note that we can also use the second qubit as the control signal by simply changing the order of the gates in the tensor product used to create the CNOT gate from $I \otimes X$ to $X \otimes I$. In matrix form, this operator is represented by a 4x4 matrix that can be written as:

$$CNOT_{0,1} = \begin{pmatrix} 1 & 0 & 0 & 0 \\ 0 & 1 & 0 & 0 \\ 0 & 0 & 0 & 1 \\ 0 & 0 & 1 & 0 \end{pmatrix}$$

3.2 One and two body Hamiltonians

Prior to the simulation of the Lipkin model, we are going to simulate two simple Hamiltonians using our VQE algoirthm, and access its performance by comparing the achieved results against the eigenvalues found using standard eigenvalue decomposition. The basic systems we consider are described below.

3.2.1 One body Hamiltonian

We define a symmetric matrix $H \in \mathbb{R}^{2\times 2}$ as:

$$H = \begin{bmatrix} H_{11} & H_{12} \\ H_{21} & H_{22} \end{bmatrix},$$

We let $H = H_0 + H_I$, where:

$$H_0 = \begin{bmatrix} E_1 & 0 \\ 0 & E_2 \end{bmatrix},$$

is a diagonal matrix. Similarly,

$$H_I = \begin{bmatrix} V_{11} & V_{12} \\ V_{21} & V_{22} \end{bmatrix},$$

where V_{ij} represent various interaction matrix elements. We can view H_0 as the non-interacting solution:

$$H_0|0\rangle = E_1|0\rangle, \quad (1)$$

and

$$H_0|1\rangle = E_2|1\rangle, \quad (2)$$

where we have defined the orthogonal computational one-qubit basis states $|0\rangle$ and $|1\rangle$.

We rewrite H (and H_0 and H_I) via Pauli matrices:

$$H_0 = EI + \Omega\sigma_z, \quad E = \frac{E_1+E_2}{2}, \quad \Omega = \frac{E_1-E_2}{2},$$

and

$$H_I = cI + \omega_z\sigma_z + \omega_x\sigma_x,$$

with $c = \frac{V_{11}+V_{22}}{2}$, $\omega_z = \frac{V_{11}-V_{22}}{2}$, and $\omega_x = V_{12} = V_{21}$. We let our Hamiltonian depend linearly on a strength parameter λ:

$$H = H_0 + \lambda H_I,$$

with $\lambda \in [0,1]$, where the limits $\lambda = 0$ and $\lambda = 1$ represent the non-interacting (or unperturbed) and fully interacting system, respectively. The model is an eigenvalue problem with only two available states.

Here we set the parameters $E_1 = 0$, $E_2 = 4$, $V_{11} = -V_{22} = 3$, and $V_{12} = V_{21} = 0.2$. The non-interacting solutions represent our computational basis. Pertinent to our choice of parameters, at $\lambda \geq \frac{2}{3}$, the lowest eigenstate is dominated by $|1\rangle$ while the upper is $|0\rangle$. At $\lambda = 1$, the $|0\rangle$ mixing of the lowest eigenvalue is 1%, while for $\lambda \leq \frac{2}{3}$, we have a $|0\rangle$ component of more than 90%. The character of the eigenvectors has therefore been interchanged when passing $\lambda = \frac{2}{3}$. The value of the parameter V_{12} represents the strength of the coupling between the two states. ([Morten, project 1])

3.2.2 Two-body Hamiltonian

We also introduce a simple system composed of two qubits, where the system can be thought of as composed of two subsystems A and B. Each subsystem has computational basis states

$$|0\rangle_{A,B} = \begin{bmatrix} 1 \\ 0 \end{bmatrix}, \quad (1)$$

$$|1\rangle_{A,B} = \begin{bmatrix} 0 \\ 1 \end{bmatrix}. \quad (2)$$

The subsystems could represent single particles or composite many-particle systems of a given symmetry. This leads to the many-body computational basis states

$$|00\rangle = |0\rangle_A \otimes |0\rangle_B = \begin{bmatrix} 1 \\ 0 \\ 0 \\ 0 \end{bmatrix}, \quad (3)$$

$$|01\rangle = |0\rangle_A \otimes |1\rangle_B = \begin{bmatrix} 0 \\ 1 \\ 0 \\ 0 \end{bmatrix}, \tag{4}$$

$$|10\rangle = |1\rangle_A \otimes |0\rangle_B = \begin{bmatrix} 0 \\ 0 \\ 1 \\ 0 \end{bmatrix}, \tag{5}$$

and finally

$$|11\rangle = |1\rangle_A \otimes |1\rangle_B = \begin{bmatrix} 0 \\ 0 \\ 0 \\ 1 \end{bmatrix}. \tag{6}$$

These computational basis states also define the eigenstates of the non-interacting Hamiltonian

$$H_0|00\rangle = \varepsilon_{00}|00\rangle, \tag{7}$$

$$H_0|10\rangle = \varepsilon_{10}|10\rangle, \tag{8}$$

$$H_0|01\rangle = \varepsilon_{01}|01\rangle, \tag{9}$$

and

$$H_0|11\rangle = \varepsilon_{11}|11\rangle. \tag{10}$$

The interacting part of the Hamiltonian H_I is given by the tensor product of two σ_x and σ_z matrices, respectively, that is

$$H_I = H_x\sigma_x \otimes \sigma_x + H_z\sigma_z \otimes \sigma_z, \tag{11}$$

where H_x and H_z are interaction strength parameters. Our final Hamiltonian matrix is given by

$$H = \begin{bmatrix} \varepsilon_{00}+H_z & 0 & 0 & H_x \\ 0 & \varepsilon_{10}-H_z & H_x & 0 \\ 0 & H_x & \varepsilon_{01}-H_z & 0 \\ H_x & 0 & 0 & \varepsilon_{11}+H_z \end{bmatrix}. \tag{12}$$

3.2.3 Von Neumann entropy for the two-body Hamiltonian

The four eigenstates of the above Hamiltonian matrix can in turn be used to define density matrices. As an example, the density matrix of the first eigenstate (lowest energy E_0, denoted as Ψ_0) is

$$\rho_0 = (\alpha_{00}|00\rangle\langle 00| + \alpha_{10}|10\rangle\langle 10| + \alpha_{01}|01\rangle\langle 01| + \alpha_{11}|11\rangle\langle 11|) \tag{13}$$

where the coefficients α_{ij} are the eigenvector coefficients resulting from the solution of the above eigenvalue problem.

We can then in turn define the density matrix for the subsets A or B as

$$\rho_A = \mathrm{Tr}_B(\rho_0) = \langle 0|\rho_0|0\rangle_B + \langle 1|\rho_0|1\rangle_B, \tag{14}$$

or

$$\rho_B = \mathrm{Tr}_A(\rho_0) = \langle 0|\rho_0|0\rangle_A + \langle 1|\rho_0|1\rangle_A. \tag{15}$$

The density matrices for these subsets can be used to compute the so-called von Neumann entropy, which is one of the possible measures of entanglement. A pure state has entropy equal to zero, while entangled states have an entropy larger than zero. The von Neumann entropy is defined as

$$S(A,B) = -\mathrm{Tr}(\rho_{A,B}\log_2(\rho_{A,B})). \tag{16}$$

We will use this definition, to measure the level of entanglement present in the system as a function of the interatction strength parameter λ.

3.3 Lipkin-Meshkov-Glick model

The Lipkin-Meshkov-Glick (LMG) model, often called Lipkin model, is a quantum model describing the collective beahvior of a large number of particles which was introduced in 1964 for the purpose of studying approximation methods used to solve many-body problems. Since its introuduction, it has become one of the standard benchmarks [Physical review C] for many-body methods in nuclear and particle physics. The model describes a system of N fermions (i.e. particles with half-integer spin values like electrons and quarks) which are distributed among two energy levels with quantum numbers σ = $\pm$1. The upper level has 2σ = +1 and energy $e_1 = e/2$, while the lower level has 2σ = -1 and energy $e_2 = e/2$. This can be visualized in the following way

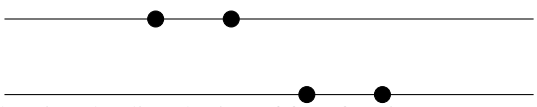

Fig. 2: Figure showing the distrubution of four fermions among two energy levels

The figure depicts two horizontal lines representing the mentioned distinct energy levels, while the dots on the lines represent four fermions that in this case are evenly distributed between these levels. Each fermion in the figure corresponds to its own substate, characterized by quantum numbers $p = 1,2,3,4$. It is important to note that in the figure, each particle occupies its own unique state. This behavior is typical of fermions, which obey the *Pauli exclusion principle* [Basdevant, p. 348], meaning that two independent fermions cannot occupy the same state at exactly the same time (Do no dwelve on this too much, this is simply the nature of reality sorrounding us).

Now the Lipkin model is described through its Hamiltonian, a matrix correpsonds to the total energy of a physicial and is fundamental plays a fundamental role in the describing the evolution of a quantum system. Here, the Hamiltonian of the system is given by

$$\hat{H} = \hat{H}_0 + \hat{H}_1 + \hat{H}_2. \tag{17}$$

where each of the the $\hat{H}_i$ can be written in terms of the creation and annihilation operators

$$\hat{H}_0 = \frac{1}{2}\varepsilon \sum_{\sigma,p} \sigma a^{\dagger}_{\sigma,p} a_{\sigma,p}, \tag{18}$$

$$\hat{H}_1 = \frac{1}{2} V \sum_{\sigma,p,p'} a^{\dagger}_{\sigma,p} a^{\dagger}_{\sigma,p'} a_{-\sigma,p'} a_{-\sigma,p}, \tag{19}$$

$$\hat{H}_2 = \frac{1}{2} W \sum_{\sigma,p,p'} a^{\dagger}_{\sigma,p} a^{\dagger}_{-\sigma,p'} a_{\sigma,p'} a_{-\sigma,p}. \tag{20}$$

Where V and W are constants, $\hat{H}_1$ represents the interaction that can move pairs of fermions between the energy levels, while $\hat{H}_2$ corresponds to the spin-exchange term, scattering one particle up and one down. These operators are in turn expressed in term of creation and annihilation operators, whose role in the context of a quantum mechanical many-body model, is the manipulation of the number of particles in specific substates. For instance, applying a creation operator to the upper energy level in Fig. 1 would increase the number of fermions in that energy level by one. One notable property of these operators is their ability to express the Hamiltonian of the Lipkin model in terms of the so-called *quasi-spin operators* and the *number operator*, where the former display behavior analogous to that of spin operators. Defining the quasi-spin operators in terms of creation and annihilation operators leads to the following equivalences

$$\hat{J}_+ = \sum_p a^{\dagger}_{p+} a_{p-}, \tag{21}$$

$$\hat{J}_- = \sum_p a^{\dagger}_{p-} a_{p+}, \tag{22}$$

$$\hat{J}_z = \frac{1}{2} \sum_{p\sigma} \sigma a^{\dagger}_{p\sigma} a_{p\sigma}, \tag{23}$$

$$\hat{J}^2 = J_+ J_- + J_z^2 - J_z. \tag{24}$$

which when substituted into the equation for the Hamiltonian $\hat{H}$, the equation for *N=2* particles is given by

$$H_I = 2\sum_p \hat{J}_z(p) - \frac{V}{2} \sum_{p\neq q} (\hat{J}_+(p)\hat{J}_+(q) + \hat{J}_-(q)\hat{J}_-(p)) - \frac{W}{2} \sum_{p\neq q} (\hat{J}_+(p)\hat{J}_-(q) - \hat{J}_-(p)\hat{J}_+(q)) \tag{25}$$

Since the quasi-spin operators exhibit behavior similar to regular spin operators, they follow the commutation relations of angular momentum (for a detailed proof, refer to [Fys5429, lecture notes week 8]). This property is of great importance because fermions, such as electrons, are particles with half-integer spin (1/2-spin). It means that a fermion possesses intrinsic spin on its own (independent of its motion) [Basdevant, p.275]. In the context of atomic systems, the energy eigenstates are intimately connected to spin [Nielsen, p.310]. Therefore, when describing a system composed of atomic particles, it is crucial to consider these internal degrees of freedom.

By utilizing quasi-spin operators, we can account for these internal degrees of freedom and incorporate them into our calculations. This allows us to rewrite the Hamiltonian of the Lipkin model in a more convenient form. Consequently, we can express the Hamiltonian matrix in terms of the Pauli operators mentioned in the previous subsection, just as we did with the one- and two-qubit Hamiltonian. This transformation facilitates the analysis and study of the Lipkin model, providing insights into its energy levels and dynamics. Before proceeding however, we are going to simplify the Hamiltonian slightly more by setting the spin-exchange term equal to zero, resulting in a dimensionless Hamiltonian

$$\hat{H} = \varepsilon \hat{J}_z - \frac{1}{2} V(\hat{J}_+ \hat{J}_+ + \hat{J}_- \hat{J}_-). \tag{26}$$

Having established the fundamental understanding of our problem and model, we move onto the encoding scheme we will apply to equation (10) for the case of the total spin *J=1,2*, corresponding to situations when the model consists of *N=2,4* particles.

3.4 Encoding in terms of Pauli matrices

As we happend to mention above, the quasi-spin operators in the expression for Hamiltonian of the Lipkin model presented in *equation (10)* can be rewritten in terms of the pauli matrices. Using the definitions of the quasi-spin $\hat{J}$ presented in [Basdevant, p.233] and [Fys5419, week8]

$$\begin{aligned} \hat{J}_x^{(n)} &\to \frac{X_n}{2}, \\ \hat{J}_y^{(n)} &\to \frac{Y_n}{2}, \\ \hat{J}_z^{(n)} &\to \frac{Z_n}{2}, \end{aligned} \tag{27}$$

where *X, Y* and *Z* are the 2x2 Pauli operators. Having done that, we still need to express the ladder operators in terms of these new mappings

$$J_\pm = J_x \pm i J_y \tag{28}$$

.

With all the necessary definitions in place, rewriting the Hamiltonian in terms of Pauli matrices becomes a straightforward task. We can substitute the appropriate terms into Equation (10) and combine the resulting operators using the Kronecker product. For the Hamiltonian with N=2, the Hamiltonian matrix can be expressed as the sum of the following tensor products:

$$H = \frac{1}{2}(Z_0 \otimes I + I \otimes Z_1) - \frac{v}{2}(X_1 \otimes X_2 - Y_1 \otimes Y_2), \tag{29}$$

The reason we are interested in rewriting the Hamiltonian a second time is because of how measurements are performed on quantum computers for particle systems. Our goal is to measure the states of the particles in basis states —0⟩ and —1⟩ (or combinations of these states). These basis states correspond to the north and south poles of the Bloch sphere (as shown in Figure 1), and interestingly, they are also the eigenstates of the Pauli Z matrix. This means that measurements are typically performed along the Z-axis. Therefore, in order to perform measurements, we need to express the Lipkin model in terms of the Pauli operators and then rotate the Hamiltonian into the Z-basis using gate equivalences.

3.5 Analytical method: Diagonalization

In solving the Lipkin model, we employ the eigendecomposition technique to find exact solutions by diagonalizing the Hamiltonian matrix. This technique relies on the fundamental property that self-adjoint operators, including the Hamiltonian, can be diagonalized. This implies the existence of orthogonal eigenvectors denoted by $\mathbf{v}$ and corresponding eigenvalues denoted by λ, satisfying the equation $\mathbf{Av} = \lambda\mathbf{v}$.

Since the Hamiltonian is a Hermitian operator [Scherer, p.38], which is self-adjoint, we can apply the eigendecomposition technique to it. By solving the characteristic equation $\det(H - \varepsilon I) = 0$, where H represents the Hamiltonian matrix and I is the identity matrix, we can determine all the eigenvalues of the Hamiltonian. These eigenvalues represent the possible energy states within the Lipkin model.

The eigendecomposition method serves as a powerful tool for obtaining precise solutions to the Lipkin model and gaining insights into its energy spectrum. By diagonalizing the Hamiltonian matrix, we can extract valuable information regarding the system's energy levels and associated eigenvectors, which describe the various states of the system.

3.6 Variational Quantum Eigensolver

The Variational Quantum Eigensolver (VQE) is a method used to estimate the ground state energy of a given Hamiltonian, such as the Lipkin Hamiltonian. This algorithm is specifically designed to handle Hamiltonian matrices that can be expressed as a sum of a polynomial number of terms involving Pauli operators [Hundt, p.242]. Examples of such Hamiltonians include the Lipkin model, Ising model, and the Harmonic Oscillator.

To estimate the ground state energy, the VQE algorithm involves three stages. In the first stage, an ansatz state is created, which is an initial state parameterized and constructed using single-qubit rotation matrices, namely R_x and R_y. These rotations correspond to rotations around the x- and y-axes of the Bloch sphere shown in Figure 1. If the system consists of multiple qubits, entanglement is introduced among the qubits of the ansatz state using Controlled-NOT gates. This is done due to the unknown level of entanglement between the qubits of the system prior to performing measurements.

In the second stage of the algorithm, measurements are performed on the system state according to *Postulate 3* for quantum measurements presented in [Nielsen, p.84-85]. During measurement, the qubit (or the wave function simulated using a qubit) collapses into one of the possible states of the system. This process is repeated a large number of times, and the resulting observations are used to approximate the probabilities associated with each possible substate of the system. Since the measurements are performed using a classical computer, it becomes easier to perform a large number of measurements and achieve accurate approximations of the probability amplitudes without the need to physically prepare particles for the system. As a result, efficient computation of the probabilities is enabled.

The last and final stage of the VQE algorithm is focused on finding the optimal parameters for our ansatz in order to minimize the expectation value produced by the algorithm. The parameters we aim to tune are the angles θ and ϕ corresponding to the rotations around the x- and y-axes of the Bloch sphere. A naive approach would involve incrementally iterating through a large number of angles to obtain a precise approximation of the ground state energy over time. However, this approach becomes inefficient for larger many-body systems with dozens of particles. Hundt proposes the use of gradient descent as a more effective method for approximating the optimal angles for our ansatz [Hundt, p. 247]. Fortunately, we can easily define the gradient of our parameterized ansatz. The expectation value can be measured in terms of the ansatz as follows:

$$\langle\psi|\hat{H}|\psi\rangle = \langle 0|R_i(\phi)^\dagger \hat{H} R_i(\phi)|0\rangle. \tag{30}$$

.

If we for instance derivate with respect to the angle ϕ, we arrive at

$$\frac{\partial}{\partial\phi}\left[\langle\psi(\theta,\phi)|H|\psi(\theta,\phi)\rangle\right] = \langle\psi(\theta,\phi)|H\left(-\frac{\iota}{2}\sigma_y|\psi(\theta,\phi)\rangle + \text{h.c.}\right) \tag{31}$$

.

Following the methodology presented in [Fys5419, week11], we arrive at a final expression for the derivative of the expectation value

$$\langle\psi|I^{\dagger}\hat{H}\left(-\frac{\iota}{2}\sigma_i|\psi\rangle\right)=\frac{1}{2}\left[\langle\psi|R_i\left(\frac{\pi}{2}\right)^{\dagger}\hat{H}R_i\left(\frac{\pi}{2}\right)|\psi\rangle-\langle\psi|R_i\left(-\frac{\pi}{2}\right)^{\dagger}\hat{H}R_i\left(-\frac{\pi}{2}\right)^{\dagger}|\psi\rangle\right]=\frac{1}{2}\left(\langle\hat{H}(\phi+\frac{\pi}{2})\rangle-\langle\hat{H}(\phi-\frac{\pi}{2})\rangle\right). \tag{32}$$

.

We will perform measurements and use the following gradient to tune our parameters to arrive at the final value.

4 Section III: Results

With the theory and methods explained, we can now present the results achieved by simulating the quanatum gates and variational quantum eigensolver.

4.1 Application of quantum gates to single qubits basis states

In the initial phase of our project, we embarked on the exploration of single qubits by preparing them in their respective basis states $|0\rangle$ and $|1\rangle$. Our objective was to investigate the effects of different quantum gates on these individual qubit systems. Notably, the outcomes observed align precisely with the theoretical predictions discussed in the earlier sections of this report. Therefore, we present the resulting states obtained by applying these gates to a qubit prepared in the state $|0\rangle$ in the table below, which serves as a comprehensive overview of our experimental findings.

Initial State	Quantum Gate	Final State
$\begin{pmatrix}1\\0\end{pmatrix}$	$I=\begin{pmatrix}1&0\\0&1\end{pmatrix}$	$\begin{pmatrix}1\\0\end{pmatrix}$
$\begin{pmatrix}1\\0\end{pmatrix}$	$X=\begin{pmatrix}0&1\\1&0\end{pmatrix}$	$\begin{pmatrix}0\\1\end{pmatrix}$
$\begin{pmatrix}1\\0\end{pmatrix}$	$Y=\begin{pmatrix}0&-i\\i&0\end{pmatrix}$	$i\begin{pmatrix}0\\1\end{pmatrix}$
$\begin{pmatrix}1\\0\end{pmatrix}$	$Z=\begin{pmatrix}1&0\\0&-1\end{pmatrix}$	$\begin{pmatrix}1\\0\end{pmatrix}$
$\begin{pmatrix}1\\0\end{pmatrix}$	$H=\frac{1}{\sqrt{2}}\begin{pmatrix}1&1\\1&-1\end{pmatrix}$	$\frac{1}{\sqrt{2}}\begin{pmatrix}1\\1\end{pmatrix}$
$\begin{pmatrix}1\\0\end{pmatrix}$	$S=\begin{pmatrix}1&0\\0&i\end{pmatrix}$	$\begin{pmatrix}1\\0\end{pmatrix}$

Table 1: Results of applying listed gates to a qubit prepared in the basis state $|0\rangle$.

During our exploration of quantum circuits, we akso conducted experiments involving the construction of an entangler circuit and the preparation of the first Bell state, $\frac{1}{\sqrt{2}}(|00\rangle+|11\rangle)$. Subsequently, we applied the Hadamard gate to the first and second qubits individually. Following this, we proceeded with the application of the CNOT(0,1) gate and concluded by reversing the order of the Hadamard and CNOT(0,1) gates, in contrast to the entangler circuit. Notably, this final operation resulted in the uncomputation of the entanglement. The comprehensive results of these operations are presented in the table below.

First Bell Pair	Quantum Operators	Resulting State
$\frac{1}{\sqrt{2}}(\|00\rangle+\|11\rangle)$	$H\otimes I$	$\frac{1}{\sqrt{2}}(\|00\rangle+\|10\rangle+\|01\rangle+\|11\rangle)$
$\frac{1}{\sqrt{2}}(\|00\rangle+\|11\rangle)$	$I\otimes H$	$\frac{1}{\sqrt{2}}(\|00\rangle+\|10\rangle+\|01\rangle+\|11\rangle)$
$\frac{1}{\sqrt{2}}(\|00\rangle+\|11\rangle)$	CNOT(0,1)	$\frac{1}{\sqrt{2}}(\|00\rangle+\|01\rangle)$
$\frac{1}{\sqrt{2}}(\|00\rangle+\|11\rangle)$	$H\otimes$ CNOT(0,1)	$\|00\rangle$
$\frac{1}{\sqrt{2}}(\|00\rangle+\|11\rangle)$	CNOT(0,1)adj$\otimes$Hadj	$\|00\rangle$

4.2 Solving one and two qubit Hamiltonians

Prior to simulating the Lipkin model using our VQE algorithm, we constructed two simple Hamiltonians representing systems comprised of one and two qubits respectively. Initially, we focused on the one-body Hamiltonian and expressed it in terms of the Pauli operators. By performing eigendecomposition, we obtained the lowest eigenvalue as a reference. Subsequently, we set up our ansatz and employed the VQE algorithm to find the ground state energy.

The figure below displays the resulting energies of the one-body Hamiltonian, with the VQE results indicated by dots in the lower plot. Notably, the VQE algorithm successfully approximates the ground state energy of this Hamiltonian. Examining the energy levels of the system, we observe that up until $\lambda = \frac{2}{3}$, the lowest eigenstate is predominantly characterized by $|0>$, while the upper eigenstate is dominated by $|1>$. However, beyond this threshold, a significant change occurs as the energy levels invert their direction, indicating an interchange in the character of the eigenvectors.

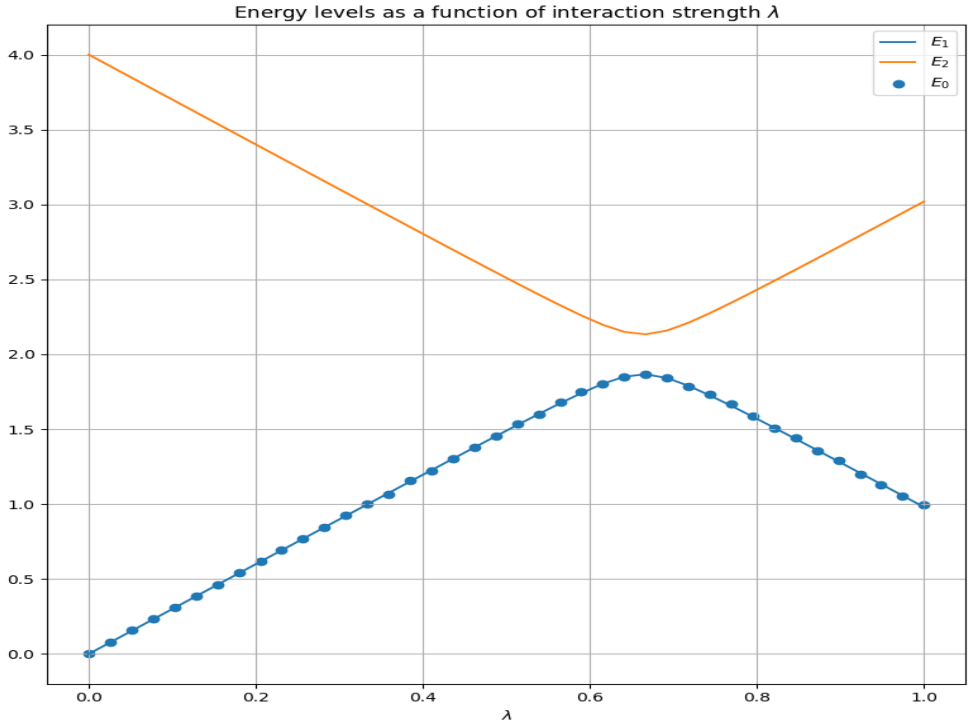

Fig. 3: Energy levels for the one-body Hamiltonian from subsection 3.2.1.

When simulating the two-body Hamiltonian, we observe that the VQE again closely resembles the analytical solution, although the approximation has slighlty less precision than in the case of the one-body Hamiltonian above. The two lewest energy levels also display a similiar behavior to that of the energy levels above, albeit for different values of the interaction strength. The energy levels are displayed in teh figure below. Another thing we notice about the VQE, is the already apparent slow down of the computations, which is caused by our representation of the operators in terms of matrices.

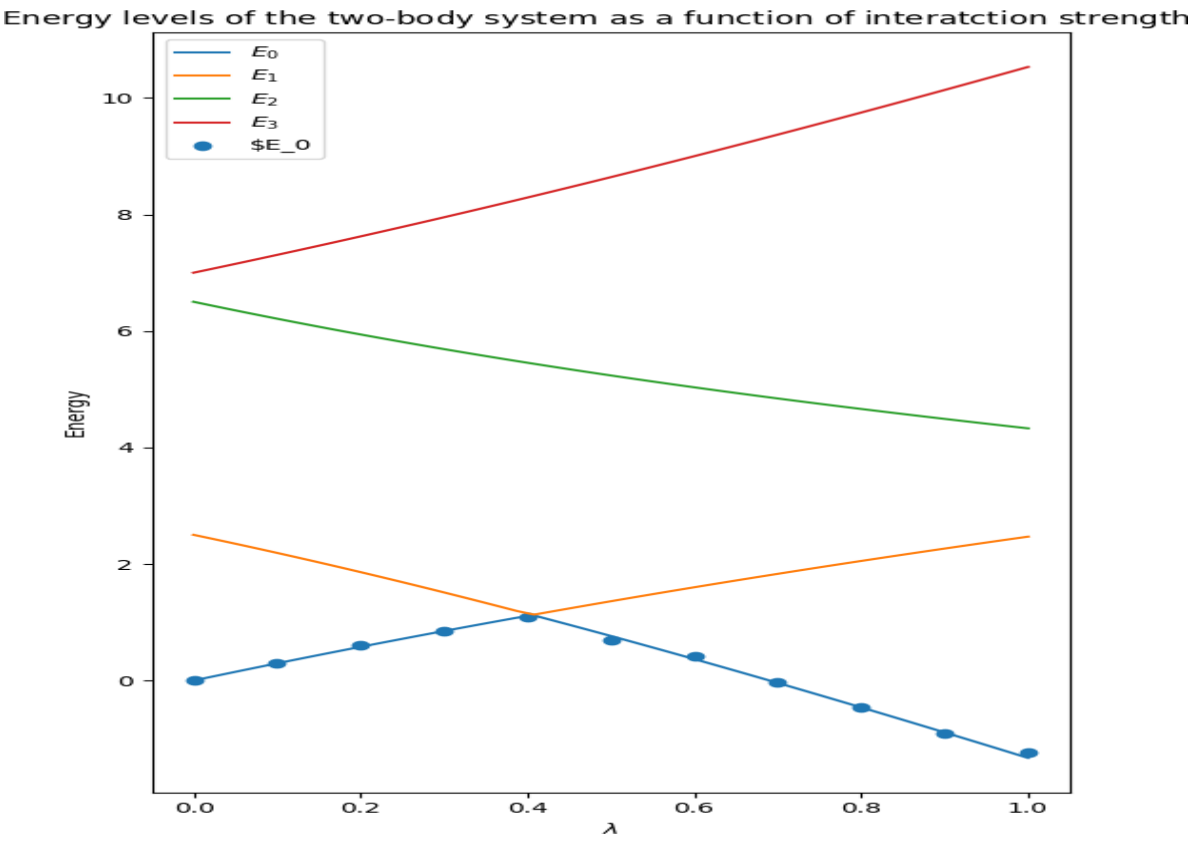

Fig. 4: Energy levels for the two-body Hamiltonian from subsection 3.2.2.

Besides the energy levels of each of the model's eigenstates, we have also measured the von Neumann entropy for the first qubit of the system in order to study entanglement within this particular system. As can be seen from Figure 5, there is a jump in entropy around the point where we have a level crossing, at around $\lambda = 0.4$. At an interaction strength of $\lambda = 0$, the many-body states are solely defined by their computational basis states. As we increase the interaction strength, the degree of mixing increases, leading to a rise in entropy. This trend continues until we reach the level crossing point, where we observe a sudden and additional increase in entropy. We observe similar behaviors for the other states. The key takeaway from this example is that entanglement is influenced by the Hamiltonian itself, including the strength of the interaction matrix elements and the non-interacting energies.

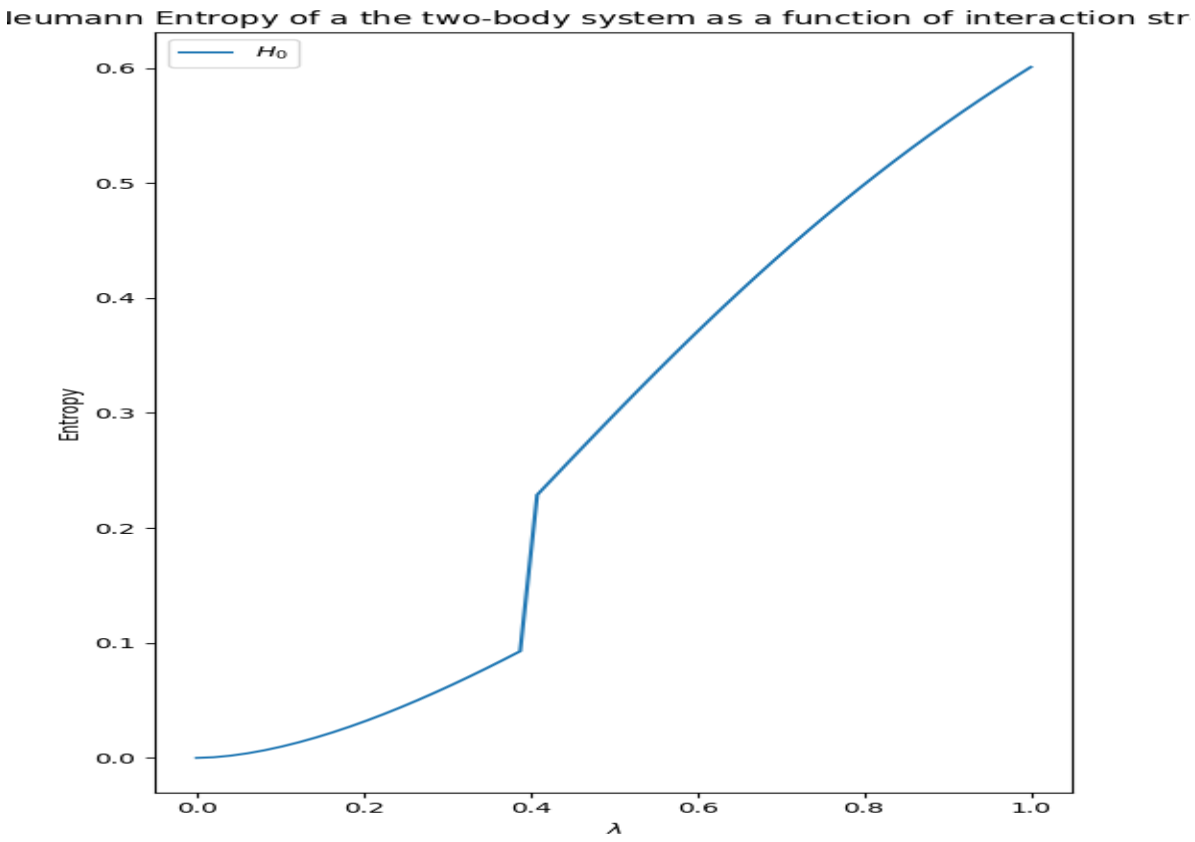

Fig. 5: Von Neumann entropy for qubit 0 of the two-body Hamiltonian of subsection 3.2.2.

4.3 Results of simulating the Lipkin model

While simulating the Lipkin model, we observed that our VQE algorithm, written purely in numpy without the utilization of any optimization libraries, started to display worse levels of precision. As a result, we improved our VQE algorithm by utilizing the *minimize* method of the *Scipy* library, resulting in visibly better precision and faster convergence times.

Starting with the case when the total spin of the Lipkin model is $J = 1$, we see that compared to the previous Hamiltonians, the energies corresponding to the eigenstates of the system display symmetries about the x-axis. Specifically, the lowest and highest eigenvalues are antisymmetric but proportional. In other words, as E_2 becomes larger as a function of V/ε, E_0 increases in the opposite (negative) direction. Interestingly, the middle eigenvalue does not evolve and remains equal to zero at all times, correctly indicating the state where each of the two fermions occupies lower and upper energy levels, respectively. The results recorded during simulation of the the Lipkin model with two fermions are shown in Figure 6.

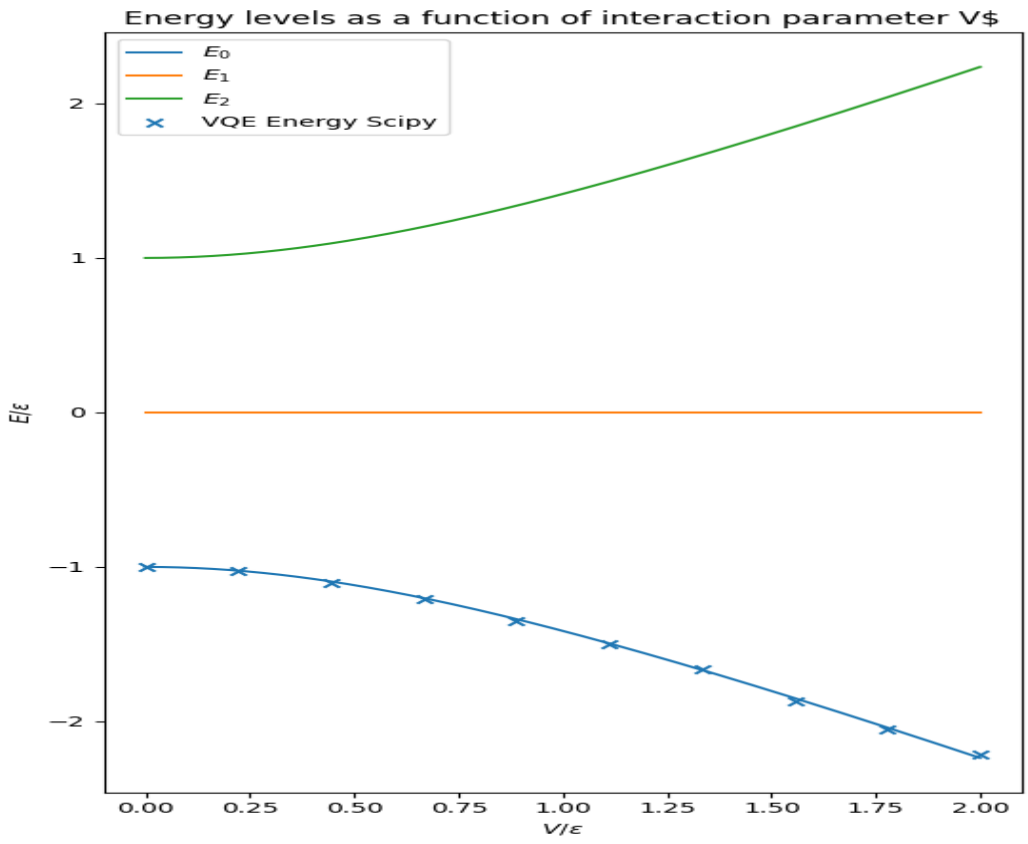

Fig. 6: Energy levels of the Lipkin model with a total spin J=1. Solution obtained using the VQE algorithm are marked with 'x'.

We observe similar symmetries when the total spin of the Lipkin model is $J = 2$. In this case, the eigenvalues above the x-axis perfectly mirror the eigenvalues below. These symmetries arise from the conservation of total spin or angular momentum, as the Lipkin model's Hamiltonian remains invariant under spin rotations. This invariance gives rise to symmetries in the energy levels and eigenstates of the system. The preservation of total spin leads to specific patterns and symmetries, such as the eigenvalues being antisymmetric but proportional, and the middle eigenvalue remaining unchanged. These symmetries are rooted in the fundamental preservation of total spin, which governs the behavior of the Lipkin model.

Moving on to the approximation of the lowest eigenvalue, we were once again able to achieve a good fit to the analytical solution (see Fig. 7, albeit at the expense of time. The algorithm required approximately 200-300 seconds to complete the computations. This highlights the point that while classical computers can be used to simulate algorithms like VQE and quantum systems with a few qubits, the increase in degrees of freedom associated with larger simulations makes it increasingly challenging. Simulating systems with more than four qubits becomes difficult, and simulating systems with more than ten qubits becomes nearly impossible, especially on standard laptops. Therefore, the limitations of classical computers in simulating large quantum systems underscore the need for quantum computers and algorithms like VQE to fully explore and understand complex quantum phenomena.

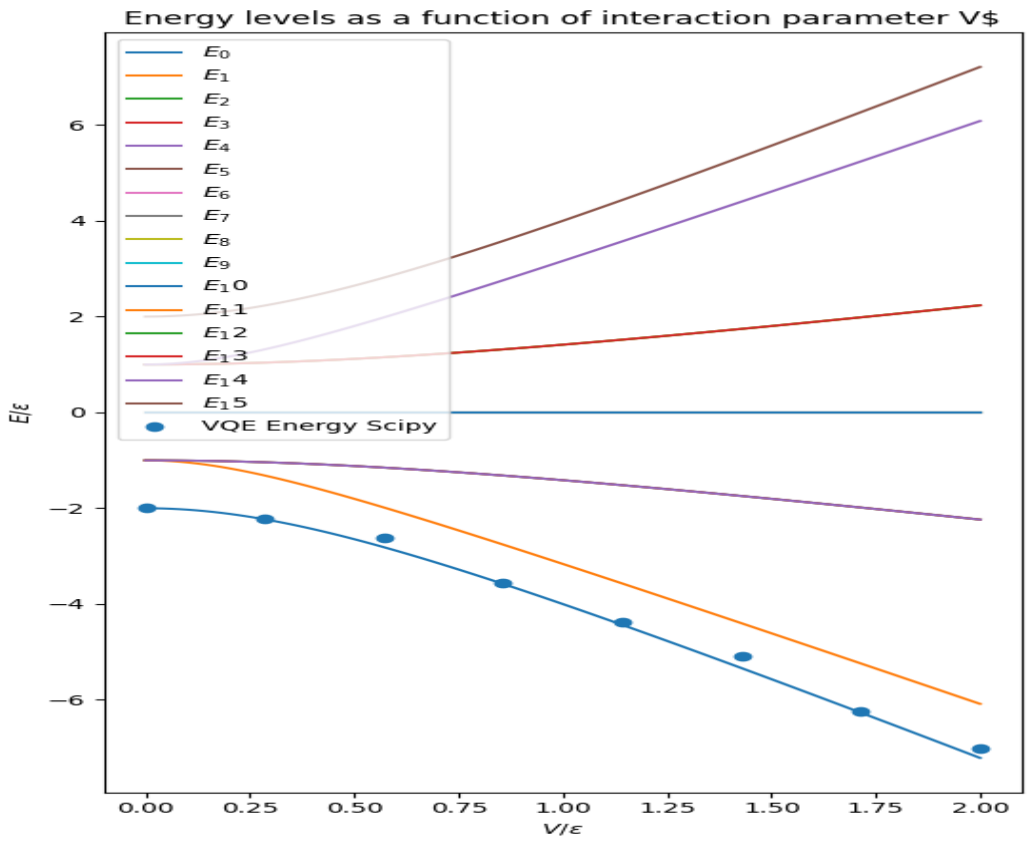

Fig. 7: Energy levels of the Lipkin model with a total spin J=2. Solution obtained using the VQE algorithm are marked with 'o'.

4.4 Summary

We initiated this project by examining the behavior of quantum gates on individual quantum bits and investigating their combination to construct more intricate circuits applicable to an arbitrary number of particles. Subsequently, we proceeded to implement the Variational Quantum Eigensolver (VQE) and develop the necessary circuits to prepare suitable ansatzes, which we coupled with the VQE to approximate the ground state energy of three distinct Hamiltonians. Beginning with a single-body Hamiltonian and culminating with the Lipkin model consisting of four fermions, we evaluated the performance of our VQE algorithm against an analytical solver, thereby gaining valuable insights.

Based on our attained results, we can assert that VQE approximates the lowest eigenvalue of the presented Hamiltonian matrices with good precision. However, it is susceptible to the curse of dimensionality stemming from the nature of qubits and the systems they compose. While the algorithm operates swiftly for systems encompassing one or two qubits, a significant reduction in computational speed becomes evident even for systems involving four particles. Consequently, further efforts must be directed toward developing more potent quantum computers. As of now, conventional analytical solvers such as eigendecomposition still outperform VQE on classical computers, and as such, remain a preferable choice of algorithm.

5 References

[Hundt, 2022] Hundt Robert (2022). Qunatum Computing for Programmers. Cambridge University Press.

[Nielsen, 2021] Nielsen Michael (2021). Qunatum Computation adm Quantum Informantion. Cambridge University Press.

[Physical review C, 2022] Manqoba Q. Hlatshwayo (2022). Simulating excited states og the Lipkin model on a Quantum Computer.

[Basdevant, 2023] Basdevant Jean-Louis (2023). Lectures on Quantum Mechanics With Problems, Exercises and Solutions. Springer Nature Switzerland.

[Scherer, 2019] Scherer Wolfgang (2019). Mathematics of Quantum Computing an Introduction. Springer Nature Switzerland.

[Morten Hjorth-Jensen, 2023] M. Hjorth-Jensen, "Week 11: VQE and project discussion," URL: https://github.com/CompPhysics/QuantumC pages/doc/pub/week11 April 2023.

[Morten Hjorth-Jensen, 2023] M. Hjorth-Jensen, "Week 8: Solving quantum mechanical problems," URL: https://github.com/CompPhysics/Q pages/doc/pub/week8, March 2023.

[Morten Hjorth-Jensen, 2023] M. Hjorth-Jensen, "Project 1: Quantum Computing and many-body problems," URL: https://github.com/Comp pages/doc/Projects/2023/Project1/pdf/Project1.pdf March 2023.